On the Nature and Extent of Intermolecular Interactions between Entrapped Complexes of $Ru(bpy)_3^{2+}$ in Zeolite Y

Milan Sykora,[†,‡] James R. Kincaid,[*,†] Prabir K. Dutta,[*,§] and Norma B. Castagnola[§]

Chemistry Department, Marquette University, Milwaukee, Wisconsin 53201-1881, and Department of Chemistry, The Ohio State University, Columbus, Ohio 43210

Received: May 15, 1998; In Final Form: September 25, 1998

A series of zeolite Y samples having different contents of entrapped $Ru(bpy)_3^{2+}$ ($Z-Ru(bpy)_3$) has been prepared. In contrast to the case in homogeneous media, in Y-zeolite the entrapped molecules cannot diffuse and the range of possible intermolecular distances between the complexes is restricted to discrete values. Because of the specific arrangement of interacting species, simplified models can be used in the study of the intermolecular interactions. The results of the present study indicate that intermolecular interactions between the entrapped complexes have a profound effect on the intensity of the electronic emission and kinetics of the excited-state depopulation. Analysis of excited-state lifetime results show that, although isolated $Z-*Ru(bpy)_3$ molecules decay to the ground state with rates comparable to that observed in aqueous solution, the decay of the excited molecules, which have another $Ru(bpy)_3^{2+}$ or $*Ru(bpy)_3^{2+}$ complex entrapped in an adjacent zeolite supercage, is much more rapid. In the case of excited-state−ground-state interaction, this effect has been attributed to the nonradiative decay enhancement, and in the case of the excited-state−excited-state interaction, it has been attributed to triplet−triplet annihilation via electron transfer.

Introduction

Intense interest and activity in the study of polypyridine complexes of divalent ruthenium has been sustained for over 2 decades because of their utility in addressing many fundamental photochemical and photophysical issues[1] and, more importantly, because of their potential value as useful components in practical solar energy conversion schemes.[2] The apparent necessity to incorporate these sensitizers into a multicomponent organized assembly, comprised of charge-relay and catalytic components, has prompted several groups to prepare and characterize chemical systems wherein such complexes are attached to, or entrapped within, various types of matrixes.[3]

The faujasitic-type Y-zeolite is an especially attractive material for entrapment of these complexes inasmuch as its structure is composed of supercages whose internal diameter is ∼13 Å. These are connected to one another, in a tetrahedral arrangement, through ∼7 Å windows to form a three-dimensional network.[4] Lunsford and co-workers[5] were the first to show that the $Ru(bpy)_3^{2+}$ complex, ∼12 Å in size, can be incorporated into Y-zeolite in a relatively straightforward manner by the so-called "ship-in-the-bottle" synthesis. We have shown[6] that zeolite-entrapped trisbipyridine ruthenium(II) is capable of sustaining relatively long-lasting charge separation upon photoinduced electron transfer to common acceptor molecules (such as viologens) which are ion-exchanged into the vacant supercages of the zeolite particles; that is, the molecular organization attainable within the zeolite framework is effective in retarding the back electron transfer.[6b]

Given these promising results, there is naturally great interest in the preparation and characterization of related materials and in gaining a deeper understanding of the effects of the zeolite framework on the inherent photophysical properties of the entrapped complexes.[7] Thus, as we have shown previously, entrapment of such complexes within the sterically constrained Y-zeolite supercages can lead to dramatic increases in ^{3}MLCT state lifetimes as a consequence of destabilization of the so-called ligand field (LF) states, from which the excited-state decay is rapid and efficient.[8]

Efforts in one of our laboratories[9] are currently focused on the construction of spatially organized multicomponent assemblies of complexes within the three-dimensional zeolitic framework. An important issue is the extent to which two complexes occupying adjacent supercages can interact. Initial efforts in one of our laboratories[3c] attempted to investigate this issue by studying the effects of increasing concentrations (loading) of the $Ru(bpy)_3^{2+}$ on the spectral and photophysical properties. However, this study failed to recognize that at high loadings of ruthenium, incomplete formation of $Ru(bpy)_3^{2+}$ was taking place. A recent study by Calzaferri and co-workers has shown that at high loading the diffusion of the bipyridine ligand is restricted, thus leading to incomplete complex formation.[10] In this study, we investigate the interactions between the zeolite entrapped $Ru(bpy)_3^{2+}$ molecules as a function of loading and have ensured that complete complexation has occurred. In contrast to other homogeneous and heterogeneous media, where ambiguities may arise because there is a continuum of possible intermolecular distances, the separation between the Y-zeolite entrapped $Ru(bpy)_3^{2+}$ molecules is restricted to discrete distances due to the crystalline nature of the matrix. The molecules can be entrapped in adjacent supercages or they can be separated from each other by a specific number of unfilled supercages. The experimental manifestations of such interactions are dramatically decreased emission intensities and evolution of complex emission decay curves as the concentration of entrapped complexes is increased. Analysis of the resulting curves

† Marquette University.
‡ Current address: Chemistry Department, University of North Carolina, CB#3290 Venable and Keenan Laboratories, Chapel Hill, North Carolina 27599.
§ The Ohio State University.

10.1021/jp982259y CCC: $18.00
Published on Web 12/29/1998

indicates that the zeolite-entrapped excited state *$Ru(bpy)_3^{2+}$ can interact with both ground- and excited-state $Ru(bpy)_3^{2+}$ complexes that occupy adjacent cages.

Experimental Section

1. Materials. The Y-zeolite was generously provided by Union Carbide Corp. The organic impurities in the zeolite were removed by oxidation under a flow of oxygen at 500 °C for 6 h.[3e] This calcined zeolite was then extensively washed with 10% NaCl and deionized water. $[Ru(NH_3)_5]Cl_3$ and 2,2′-bipyridine (bpy) were purchased from Aldrich Chemical Co. The bpy was sublimed prior to use.

2. Preparation of the Zeolite-Entrapped Z−Ru(bpy)$_3$. The $Z-Ru(bpy)_3^{2+}$ was prepared by a method described previously[7] that is based on the work of Lunsford and co-workers.[5] Briefly, 3 g of calcinated Na−Y-zeolite was suspended in 500 mL of cold deionized water. The pH of the suspension was then slowly adjusted to pH = 5.2−5.5 with 0.1 M HCl solution, and subsequently, the appropriate amount of $[Ru(NH_3)_6]Cl_3$ (depending on desired load of $Ru(bpy)_3^{2+}$) was added. The suspension was then stirred at 4 °C overnight. The $Z-Ru(NH_3)_6^{3+}$ was then quickly filtered and allowed to dry in air. The dry $Z-Ru(NH_3)_6^{3+}$ was then mechanically mixed with a 50-fold excess (with respect to $[Ru(NH_3)_6]^{3+}$) of solid bpy. The mixture was then transferred to a 15 mm × 10 cm Pyrex tube fitted with a vacuum stopcock. The tube was evacuated, subsequently filled with nitrogen twice, and finally evacuated at 10^{-3} Torr for 1 h. The evacuated tube containing the reaction mixture was then immersed into a 200 °C oil bath and heated at this temperature for several days. The mixture was allowed to cool to room temperature, and the $Z-Ru(bpy)_3^{2+}$ was washed with 3 L of 10% (w/v) NaCl, 0.5 L of deionized water, and 0.5 L of 95% EtOH. Excess (unreacted) bpy was removed by extensive Soxhlet extraction with 95% EtOH. During the Soxhlet extraction (typically 10−20 days depending on the $Ru(bpy)_3^{2+}$ load and volume of the extractor), the EtOH washings were periodically checked for the presence of bpy by UV−vis spectroscopy (monitoring the band at ∼286 nm) until no traces of bpy could be detected. Finally, the solid $Z-Ru(bpy)_3^{2+}$ was air-dried at room temperature.

3. Liberation of Z−Ru(bpy)$_3^{2+}$ from the Zeolite Matrix. A previously described "hydrofluoric acid" method was used.[7a] A 0.05 g sample of $Z-Ru(bpy)_3^{2+}$ was suspended and stirred in 4 mL of a solution composed of 20 parts of H_2O and 1 part of concentrated HF. After a few minutes, all the zeolite dissolved and a clear orange solution was obtained. The pH was adjusted to pH = 7 with 2 M NaOH and the sample was centrifuged to remove the precipitated solid. The orange solution, drawn off with a Pasteur pipet, was used directly for measurement of the absorption spectrum.

To determine the extent of contamination by trace organic impurities present in the zeolite even after extensive Soxhlet extraction with EtOH (vide infra) the following procedure has been employed. The most concentrated zeolitic sample (1 Ru/1.9 cages) was treated with diluted HF as described in the previous paragraph. A 5 mL portion of the resulting solution was then extracted with 5 mL of CH_2Cl_2. The UV−vis spectra of both the aqueous and organic phases were then measured in the region 220−820 nm. Neither of the extracts was further diluted prior the absorption measurements.

Physical Measurements

1. X-ray Fluorescence. The concentration of $Ru(bpy)_3^{2+}$ in Y-zeolite was determined nondestructively by X-ray fluorescence as described previously.[3c] The calibration curve was constructed using a series of $Z-Ru(NH_3)_6^{3+}$ samples with four different concentrations of ion-exchanged $Ru(NH_3)_6^{3+}$.

2. Electronic Absorption Spectra. Electronic absorption spectra were obtained with a Hewllett-Packard model 8452A diode array spectrometer. Spectra were obtained in the absorbance mode using a 1 cm quartz cuvette.

3. Diffuse Reflectance Spectra. The diffuse reflectance spectra were recorded on a Shimadzu 265 spectrometer equipped with a Harrick diffuse reflectance attachment. The $Z-Ru(bpy)_3^{2+}$ samples were measured as such and plain Na−Y-zeolite was used as the reference. The spectra, recorded in the transmittance mode (with resolution of 1 nm), were numerically Kubelka−Munk corrected using the facilities of Grams32 software.

4. Electronic Emission Spectra. The $Z-Ru(bpy)_3^{2+}$ samples were transferred into 5 mm i.d. NMR tubes, degassed at $\sim 10^{-4}$ Torr overnight, exposed to vapors of degassed (3 × freeze−pump−thaw) deionized water, and finally sealed inside the NMR tube. Electronic emission spectra were obtained using a conventional Raman spectrometer (Spex model 1403 double monochromator equipped with a Spex model DM1B controller and a Hammamatsu R928 photomultiplier tube, resolution 1 nm) with 457.9 nm excitation from a Spectra-Physics model 2025-05 argon ion laser set in the constant power mode, with the power at the sample being ∼2mW. The spinning 5 mm i.d. NMR tube was illuminated by a laser beam focused through a glass lens, and the emission from the sample was collected with a conventional two-lens collecting system.

5. Excited-State Lifetimes. The samples for lifetime measurements were freshly degassed following the procedure used for emission measurements. The third harmonic (354.7 nm; fwhm = 12 ns) of a Quanta-Ray (Spectra-Physics) model GCR-11 Nd:YAG laser, operated at 20 Hz with the beam defocused (∼2 mm diameter), was used as the excitation source for the lifetime measurements. The light emitted from the sample in the spinning NMR tube was transferred through collecting and transferring lenses to a SPEX 340S spectrometer equipped with an RCAC31034A-02 photomultiplier tube with ∼1800 V of applied voltage. The PMT output signal was directed to a LeCroy 9450A dual 300 MHz oscilloscope. The temperature change in the laboratory did not exceed ±0.3 K during the measurement. Typically, 3000 scans of the emission decay curve were averaged and transferred to the computer. The curves (extending to times greater than 4 times the longest lifetime) were then fitted by an appropriate kinetic model. Initially, several data sets, at different concentrations and excitation powers, were analyzed by both locally written software with deconvolving capabilities (to estimate the contribution of the instrument response function (IRF) to extracted parameters) and commercial software (PSI-Plot) without the deconvolving capabilities. Since there was no apparent difference in the quality of the fit or the absolute values of the extracted parameters, the commercial software has been used to analyze the complete set of data because of its superior statistical analysis capabilities. Despite such testing of the data via numerical deconvolution, the extracted lifetime and the relative contribution of the short component should be taken as aproximate values, considering the temporal width of the laser pulse. Both computer programs were based on the Marquardt−Levenberg algorithm.

Results

1. Characterization of Z−Ru(bpy)$_3^{2+}$. In this study, a series of six $Z-Ru(bpy)_3$ samples having increasing contents of

TABLE 1: Summary of Diffuse Reflectance and Emission Spectra for Z−$Ru(bpy)_3^{2+}$ Series

concentration of $Ru(bpy)_3^{2+}$ in Y-zeolite[a]			absorption	emission		
μmol Ru/1 g Y−Z	mol dm^{-3}	no. supercages/1Ru	A_{max} (I_A)[b]	E_{max}[c]	I_{rel} (st. dev.)[d]	I_{rel}/I_A
6.92 (±0.05)	0.013	66.7	455 (0.6)	620	1.00 (±0.03)	1.82
15.56 (±0.05)	0.030	29.7	455 (1.1)	620	0.94 (±0.03)	0.88
32.9 (±0.2)	0.063	14.0	454 (2.6)	620	0.93 (±0.05)	0.36
61.3 (±0.2)	0.118	7.5	454 (3.1)	621	0.92 (±0.04)	0.29
104.6 (±0.9)	0.201	4.4	452 (5.3)	623	0.87 (±0.05)	0.16
239 (±3)	0.460	1.9	449 (10.1)	623	0.39 (±0.04)	0.04

[a] Concentrations as determined by X-ray fluorescence; for transformation of concentrations from μmol $Ru(NH_3)_6^{3+}$ per 1 g zeolite to concentration expressed in mol dm^{-3} and number of cages per one Z−$Ru(bpy)_3^{2+}$ molecule the density $d = 1.92$ g/cm^{-3} and the volume of unit cell $V = 15\,000$ Å^3 was used.[4] [b] Observed absorption maximum for the $^1GS \rightarrow {}^1MLCT$ transition and corresponding absorption (I_A), in Kubelka−Munk units at A_{max}. [c] Observed maximum for $^3MLCT \rightarrow {}^1GS$ transition, from spectra in Figure 3. [d] Relative emission intensities and corresponding standard deviations as determined from series of independent measurements; the actual spectral data are shown in Figure 3.

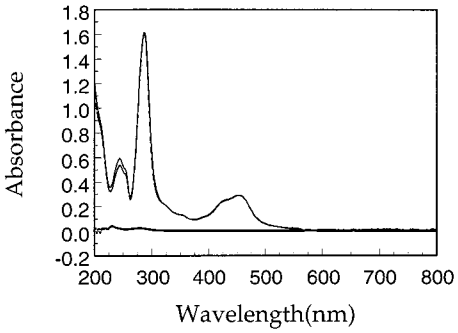

Figure 1. UV−visible spectrum of $Ru(bpy)_3^{2+}$ extracted from Z−$Ru(bpy)_3$ (1/1.9) by HF method and subsequently extracted with CH_2Cl_2: UV−vis spectrum of the extracted aqueous phase (solid line); UV−visible spectrum of the extracted organic phase (dotted line); UV−visible spectrum of independently synthesized $[Ru(bpy)_3]Cl_2$ in aqueous solution (dashed line).

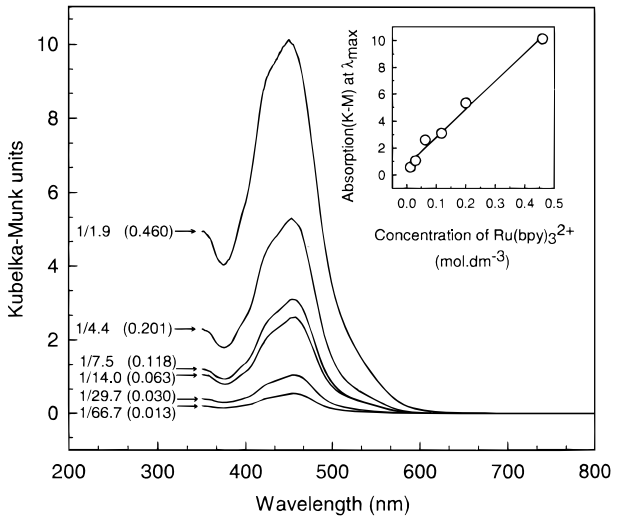

Figure 2. Diffuse reflectance of the MLCT region for the Z−$Ru(bpy)_3$ series. The concentrations are expressed in number of $Ru(bpy)_3^{2+}$ complexes per number of supercages (in parentheses, corresponding molar concentrations). The inset shows the variation in the absorbance (in Kubleka−Munk units) at the absorption maximum as a function of Z−$Ru(bpy)_3$ concentration (as determined independently by X-ray fluorescence).

entrapped $Ru(bpy)_3^{2+}$ has been prepared. The exact concentrations of the entrapped complex for each sample, as determined by X-ray fluorescence measurements, are summarized in Table 1. To study the interactions between the zeolite entrapped $Ru(bpy)_3^{2+}$ molecules, it is extremely important that the samples studied are not contaminated with trace impurities. Calzaferri and co-workers[10] observed that, at very high loads of the entrapped complex, the most abundant contaminant in the product of the Z−$Ru(bpy)_3$ synthesis is a reaction intermediate, Z−$Ru(bpy)_2$. With the increase in the total load of the entrapped complex, the diffusion of the bpy ligand through the zeolite during the reaction becomes significantly obstructed and thus not all $Ru(NH_3)_6^{2+}$ centers are converted into $Ru(bpy)_3^{2+}$. To minimize the risk of contamination with $Ru(bpy)_2^{2+}$, long reaction times and large excesses of bpy were used in the synthesis of all samples studied here. Inasmuch as the risk of contamination is most critical for highly concentrated samples, the UV−vis spectra of the solution prepared by dissolving the most concentrated Z−$Ru(bpy)_3$ sample (load 1/1.9) in HF were compared with that of an aqueous solution of independently synthesized $[Ru(bpy)_3]Cl_2$. To determine the extent of contamination, not only by inorganic (e.g., Z−$Ru(bpy)_2$) but also organic impurities (e.g., unreacted ligand or byproducts), the HF extract of the zeolitic sample was further extracted with CH_2Cl_2 and the absorption spectra of the organic phase was measured. In Figure 1 are compared the absorption spectra of both the aqueous and organic phase of the zeolitic extract (of the sample with load 1/1.9) with the UV−vis spectrum of an aqueous solution of the independently prepared $[Ru(bpy)_3]Cl_2$. The spectra of the $[Ru(bpy)_3]Cl_2$ and the aqueous phase of the HF extract are superimposable in the visible region (indicating no contamination with Z−$Ru(bpy)_2$) and nearly superimposable in the UV region (indicating virtually no contamination by absorbing organic impurities). In the absorption spectrum of the CH_2Cl_2 extract, a very weak band (absorbance ~0.02) was detected. On the basis of the GC-MS analysis, this weak feature has been attributed to trace amounts of unreacted bpy trapped in the zeolite matrix. Assuming the same optical density for free and coordinated bpy, the molar ratio of $Ru(bpy)_3^{2+}$ to bpy in this sample is approximately 100:1. No absorption band has been detected in the organic extract of the samples with lower total content of the $Ru(bpy)_3^{2+}$ (load ≤ 1/4.4). This is an expected result considering that the smaller amount of the complex allows more efficient removal of the bpy from the zeolite supercages during the Soxhlet extraction. Thus, these results provide convincing evidence that (1) under the conditions used in this work the formation of Z−$Ru(bpy)_2$ contaminant can be prevented up to a load of the complex 1 $Ru(bpy)_3^{2+}$/1.9 supercages and (2) the extensive Soxhlet extraction is an efficient procedure for the removal of excess of unreacted bpy and other organic impurities.

2. Diffuse Reflectance. Figure 2 shows the diffuse reflectance (DR) spectra of the zeolite-entrapped $Ru(bpy)_3^{2+}$ samples. The lack of a band or a shoulder at ~490 nm indicates no contamination of any of the samples by reaction intermediates such as Z−$Ru(bpy)_2$. This result is consistent with the results summarized in previous section. Also shown in Figure 2 (inset) is the variation in the intensity of the peak of the MLCT band

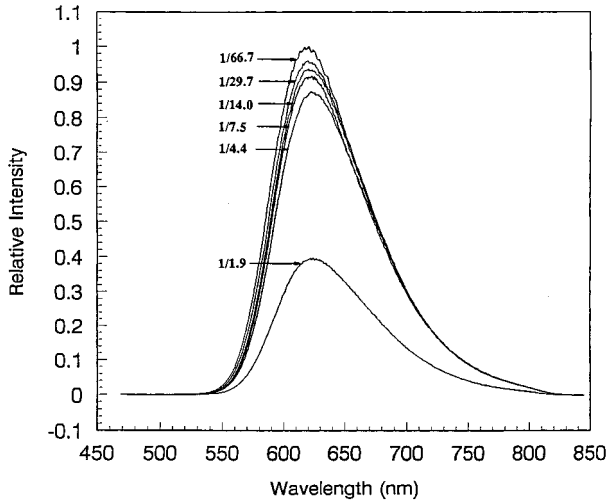

Figure 3. Electronic emission spectra for the Z−Ru(bpy)$_3$ series. The concentrations expressed in number of Ru(bpy)$_3^{2+}$ complexes per number of supercages. Spectra are not corrected for variation in the chromophore concentration or for the detector response.

as a function of the complex loading, determined by X-ray fluorescence. Within the concentration range of Ru(bpy)$_3^{2+}$ used in this study, Beer's law seems to be valid. Upon careful inspection of the DR spectra, a small blue shift, ∼5 nm (instrument resolution is 1 nm), of the MLCT was detected with the increase of the concentration of the entrapped complex over the studied concentration range (0.01 to ∼0.5 mol dm^{-3}; i.e., 1 Ru/66.7 cages to 1 Ru/1.9 cages). The positions of the maxima of the MLCT band for the studied samples as extracted from DR are summarized in Table 1.

3. Electronic Emission. In Figure 3 are shown the emission spectra of the zeolite entrapped complexes. A small (∼3 nm; resolution of 1 nm) red shift for the Z−Ru(bpy)$_3^{2+}$ samples was observed over the concentration range of 0.01−0.5 mol dm^{-3}. The position of the emission maxima and the corresponding relative emission intensities are summarized in Table 1. The most striking observation is the significant decrease of the emission intensity with increasing Ru(bpy)$_3^{2+}$ concentration. Thus, there is about a 2.5-fold decrease in intensity of the emission band when comparing the most dilute (0.013 mol dm^{-3} or 1 Ru/66.7 cages) and the most concentrated (0.46 mol dm^{-3} or 1 Ru/1.9 cages) samples, while at the same time there is a linear increase in the total amount of light absorbed with increasing concentration in the same concentration range (Figure 2). When normalized to the amount of light absorbed, i.e., the ratio of the emission intensity at ∼620 nm to the absorbance (in Kubelka−Munk units) at ∼450 nm, the relative decrease in the emission intensity for the most concentrated sample (1.9 supercages/Ru) as compared to the most dilute sample (66.7 supercages/Ru) is 45-fold (0.04 vs 1.8 respectively; see Table 1).

4. Excited-State Lifetimes. In Figure 4 is shown the dependence of the emission decays on the load of the entrapped complex. As is apparent from the traces shown in Figure 4a, the rate of the emission decay increases dramatically with increasing concentration, within the concentration range studied. The traces in Figure 4b show the same data plotted on the logarithmic scale. Even though at longer times all traces are linear, at times below 200 ns there are obvious deviations from linearity for the highly loaded samples. Variations in the emission decays of Z−Ru(bpy)$_3^{2+}$ induced by changes in concentration were studied also as a function of the power of the excitation light. Variations in the appearance of the emission

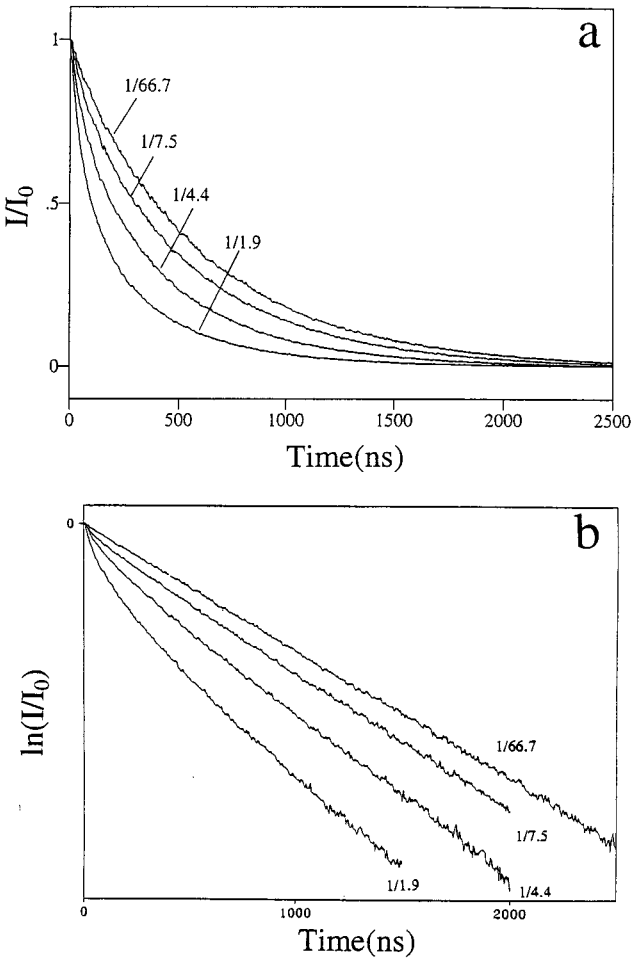

Figure 4. (a) Normalized emission decays for Z−*Ru(bpy)$_3$ as a function of concentration at excitation power 1 mW, i.e., 0.05 mJ/pulse. Loading levels as indicated in the figure (i.e., 1/1.9 corresponds to 1 Ru(bpy)$_3^{2+}$/1.9 supercages). (b) Same data plotted on a semilogarithmic scale.

decays with changes in excitation power for the sample containing 1 Ru/4.4 supercages are shown in Figure 5. From the figure, it is evident that the emission decays more rapidly as the excitation power increases. The traces in Figure 5b, plotted on the logarithmic scale, indicate that the deviations from linearity at times below 200 ns are also enhanced with an increase in the power of the exciting light. The experimental data thus indicate that simple first-order kinetics is followed in the emission decay of Z−*Ru(bpy)$_3^{2+}$ only at low concentrations (≤1/60) and low excitation powers (≤0.5 mW).[11]

Discussion

The structure of the aluminosilicate framework of a single zeolite Y supercage is shown in Figure 6A. Each Y-zeolite supercage, which is approximately 13 Å in diameter, is connected to four tetrahedrally arranged neighboring cages via ∼7 Å windows. This tetrahedral pattern is repeated throughout the zeolite particle, whose typical size is several micrometers (corresponding to ∼10^9−10^{10} supercages). A unit cell of Y-zeolite, composed of eight supercages, contains approximately 250 molecules of water and 56 Na$^+$ ions distributed over the free volume of large supercages and smaller β-cages.[4]

The first step toward synthesis of the zeolite-entrapped Ru(bpy)$_3^{2+}$ (Z−Ru(bpy)$_3$) is the ion exchange of the [Ru(NH$_3$)$_6$]$^{3+}$ precursor into the zeolite, partially replacing the Na$^+$ ions. The amount of ion-exchanged ruthenium hexammine ion then

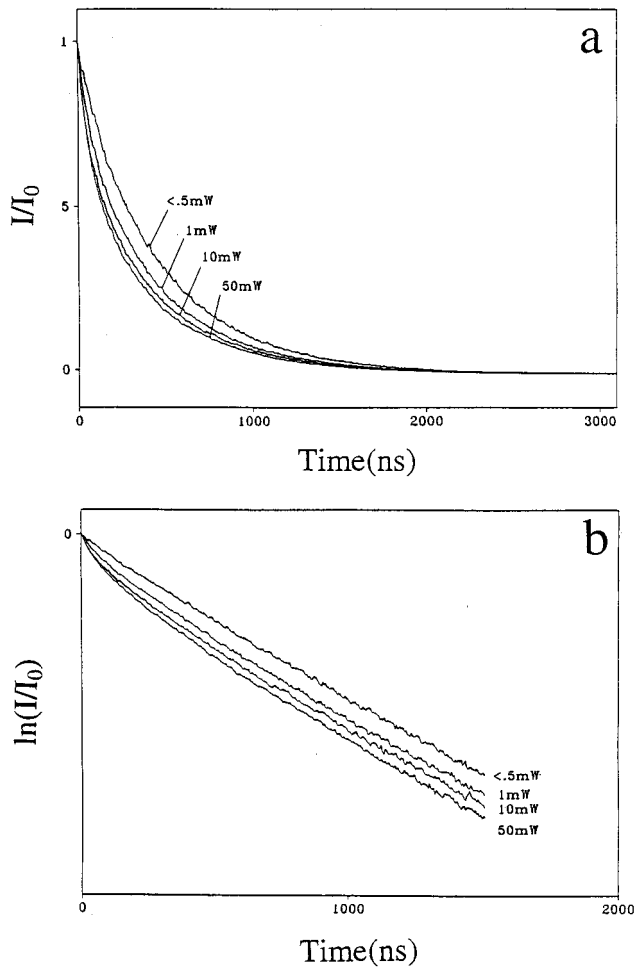

Figure 5. (a) Normalized emission decays for Z−*$Ru(bpy)_3$ (load of ∼1 Ru/4.4 supercages) as a function of power. (b) Same data plotted on a semilogarithmic scale.

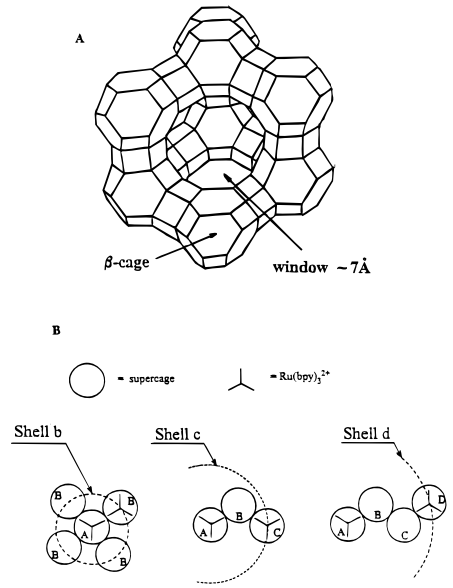

Figure 6. (a) Structure of single supercage of Y-zeolite. (b) Schematic diagram of the shell model of the Y-zeolite structure.

determines the concentration (load) of the final product inside the zeolite. Assuming a random distribution of $[Ru(NH_3)_6]^{3+}$ ions within the zeolite during the ion exchange process, the intermolecular distance between the entrapped Z−$Ru(bpy)_3^{2+}$ molecules can be expected to decrease incrementally with an increase in the concentration of Z−$Ru(bpy)_3^{2+}$. While in solutions (and in most heterogeneous media) at any concentration a continuum of intermolecular distances is possible, the regular structure of Y-zeolite restricts the possible intermolecular separations to discrete values, defined by the number of unfilled supercages separating any pair of entrapped molecules. To take into account this discrete nature of Y-zeolite and thus facilitate a quantitative analysis of the observed experimental data in terms of intermolecular interactions, a structural model for the arrangement of the $Ru(bpy)_3^{2+}$ in the Y-zeolite has been developed.

TABLE 2: Structural Model for $Ru(bpy)_3^{2+}$-Loaded Y-Zeolite

shell	no. cages/shell	shell radius (Å)	$Ru(bpy)_3^{2+}$ to $Ru(bpy)_3^{2+}$ estimated distance (Å)
a	1		
b	4	13.00	∼1
c	12	21.23	∼9
d	12	24.89	∼13
e	6	30.02	∼18
f	12	32.72	∼21
g	24	36.77	∼25
h	12	39.00	∼27

1. Structural Model of Z−Ru(bpy)$_3$. Given the known size and regular tetrahedral arrangement of Y-zeolite supercages, for various loading levels it is possible to calculate the allowable intermolecular distances between the entrapped molecules as well as to estimate what fractions of the entrapped $Ru(bpy)_3^{2+}$ molecules are separated by 0, 1, 2, ... unfilled supercages. To obtain this information, the model schematically shown in Figure 6B has been developed. In the first step, we have considered an arbitrary supercage within the zeolite particle and marked it as supercage "A". The cage "A" is tetrahedrally surrounded by four neighbors—"B". Assuming that the diameter of the (approximately spherical) cavity of a supercage is ∼13 Å, the distance (center "A" to center "B") is identical for all four "B" cages and equal to ∼13 Å. The centers of the four "B" cages, equidistant from the center of "A", thus form a shell "b" with a diameter of 13 Å. Each of the four cages in shell "b" (all adjacent to cage "A") has three additional neighbors, the centers of which are also equidistant from the center of "A", and these comprise a 12-membered shell "c". The distance from the center "A" to the center of any of the "C" cages (shell "c" diameter) can be calculated using basic geometrical considerations to be 21.23 Å. Considering the repeating tetrahedral pattern, this model can be extended to additional "shells", and for each shell, the number of cages and the corresponding shell diameter can be calculated. The results of such calculations for the first eight shells are summarized in Table 2. The table also includes estimated (periphery-to-periphery) distances between two $Ru(bpy)_3^{2+}$ molecules, one of which is arbitrarily chosen to be entrapped in supercage "A" and the second one of which is immobilized in one of the supercages of shell "b", "c", "d", etc. The distances shown in the table were calculated simply by subtracting twice the radius of the $Ru(bpy)_3^{2+}$ molecule (as obtained from X-ray crystallographic data[12]) from the calculated radius for a particular shell, with the radius of the $Ru(bpy)_3^{2+}$ being considered the distance from the Ru center to the 4- or 4′- hydrogen (equal to ∼6 Å[12]).

The distribution of the $Ru(bpy)_3^{2+}$ ions within the Y-zeolite at any given load of the complex can be calculated using the following approach. At a load of 1 $Ru(bpy)_3^{2+}$/66.7 supercages, the probability of any randomly selected cage within the sample being occupied with a $Ru(bpy)_3^{2+}$ molecule is 1/66.7 = 0.015. Consequently, the probability that any randomly selected cage

TABLE 3: Distribution of $Ru(bpy)_3^{2+}$ in Y-Zeolite as a Function of $Ru(bpy)_3^{2+}$ Load

load	shell (no. cages/shell)							
(Ru/no. cages)	b (4)	c (12)	d (12)	e (6)	f (12)	g (24)	h (12)	accounted for
1/66.7	5.86%	15.61%	13.02%	5.68%	9.92%	15.18%	5.76%	(71.02%)
1/29.7	12.80%	29.39%	19.48%	7.12%	10.52%	11.60%	3.06%	(93.97%)
1/14.0	25.65%	43.79%	18.00%	4.51%	4.74%	2.75%	0.33%	(99.77%)
1/7.5	43.58%	46.29%	8.31%	1.05%	0.63%	0.13%	0.00%	(100.00%)
1/4.4	64.35%	34.04%	1.54%	0.06%	0.01%	0.00%		(100.00%)
1/1.9	94.97%	5.03%	0.00%					(100.00%)

will not be occupied with a $Ru(bpy)_3^{2+}$ complex is $1 - 0.015 = 0.985$ (i.e., each zeolite cage can be visualized as being 1.5% full and 98.5% empty).

Now, considering a single supercage ("A") within the sample, which is occupied by a $Ru(bpy)_3^{2+}$ ion, the probability that any of the remaining cages (including cages immediately surrounding the cage "A", i.e., cages of shells "b", "c", ...) is not occupied by $Ru(bpy)_3^{2+}$ is expected to be, as calculated before, 0.985. Thus, the probability that all four "B" cages surrounding the cage "A" are "empty" (not occupied by $Ru(bpy)_3^{2+}$) is $0.985^4 = 0.941$. Consequently, the probability that the shell "b" is occupied by *at least one* $Ru(bpy)_3^{2+}$ is $1-0.941 = 0.0587$ or 5.87%; that is, shell "b" can be visualized as being 5.87% full. These considerations can be extended to determination of the populations of the remaining shells.[13] and the distribution of $Ru(bpy)_3^{2+}$ molecules within the zeolite at any particular load can be estimated. The calculated distributions, within the first eight shells, for the $Z-Ru(bpy)_3^{2+}$ samples studied here are summarized in Table 3.

As expected, at low loading levels, the entrapped ions are relatively evenly distributed throughout the zeolite particle. Thus, for example, at the lowest loading level (1/66.7), from any randomly selected 100 $Ru(bpy)_3^{2+}$ ions, 5−6 (occupying shell "b") will be members of an adjacent pair, 15−16 (occupying shell "c") will be separated from the nearest $Ru(bpy)_3^{2+}$ ion by one empty supercage, 13 (occupying shell "d") will be separated from the nearest $Ru(bpy)_3^{2+}$ ion by two empty supercages, etc. At higher concentrations, the likelihood of finding a $Ru(bpy)_3^{2+}$ molecule that is isolated from its nearest neighbor by one or more unoccupied shells rapidly decreases. Ultimately, at the highest loading (1 $Ru(bpy)_3^{2+}$ per 1.9 supercages), ∼95% of the $Ru(bpy)_3^{2+}$ ions have at least one $Ru(bpy)_3^{2+}$ neighbor within the four surrounding supercages; that is, there is only ∼5% chance of finding a $Ru(bpy)_3^{2+}$ molecule surrounded by four supercages that are not occupied by another $Ru(bpy)_3^{2+}$.

There are two main limitations of the model discussed above that must be kept in mind while analyzing the experimental data. First, the model is based on purely statistical considerations and thus assumes a truly random distribution of $Ru(bpy)_3^{2+}$ molecules within the Y-zeolite matrix. This assumption may not be strictly valid, especially at very high loads where steric and electrostatic effects could lead to a nonhomogeneous distribution of $[Ru(NH_3)_6]^{3+}$ ions during the ion exchange. However, as has been shown by Calzaferri and co-workers,[10] the assumption of a homogeneous distribution of $Ru(bpy)_3^{2+}$ ions "holds" up to loads of 1 $Ru(bpy)_3^{2+}$/2 supercages, i.e., the highest loading level studied in this work. Second, in the model it is assumed that every supercage is surrounded by four neighboring supercages. However, this is not true for some of the supercages near the surface of the zeolite particle that can be adjacent to three, two, or even one supercage. The $Ru(bpy)_3^{2+}$ ions occupying these cages are less likely to be members of an adjacent multiplet; in other words, they have a greater chance of being "isolated" than do $Ru(bpy)_3^{2+}$ ions located inside the zeolite particle. While at low $Ru(bpy)_3^{2+}$ loads, the occupation of surface cages will have a small effect on the ratio of "isolated" vs "adjacent" ions, at high loads the theoretical model overestimates the fraction of "adjacent" ions and underestimates the fraction of "isolated" ions.

2. Analysis of Intermolecular Interactions. *Electronic Absorption and Emission.* Martin and co-workers[14] studied the effect of changes in concentration on absorption spectra of $Ru(bpy)_3^{2+}$ incorporated in layered colloidal ZrPS (zirconium phosphate sulfenyl phosphonate). The increase in the loading of $Ru(bpy)_3^{2+}$ in ZrPS resulted in a significant (>30 nm) red shift in the position of the $Ru(bpy)_3^{2+}$ MLCT band. The shift was attributed to the intermolecular interactions between ZrPS-incorporated $Ru(bpy)_3^{2+}$ complexes. Our diffuse reflectance results do not show significant shifts in the position of the MLCT band (only minor blue shifts are observed; see Table 1). Although the quantitative comparison of our data with the results obtained for ZrPS system is not straightforward,[15] clearly the concentration effect on the position of the MLCT absorption seems to be more dramatic in the ZrPS system than in zeolites.

The effect of concentration on the position of the emission maximum of the $Ru(bpy)_3^{2+}$ complex in aqueous solution and incorporated in ZrPS has also been studied by Martin et al.[14] A 6 nm red shift (622−628 nm) was observed as the concentration was increased from 1×10^{-2} to 6×10^{-2} mol dm^{-3} in aqueous solution, and a similar red shift was observed for the ZrPS samples over a comparable concentration range. The emission from $Z-Ru(bpy)_3$ shows the same tendency, although in zeolites, in the concentration range 1×10^{-2} to 46×10^{-2} mol dm^{-3}, the observed shift is much smaller, i.e., ∼3 nm (see Table 1). Thomas and Milosavijevic[16] studied the effect of concentration on the emission intensity of $*Ru(bpy)_3^{2+}$ adsorbed onto cellophane film. They observed a steady increase in intensity with concentration over the concentration range $10^{-4}-10^{-2}$ mol dm^{-3}. At concentrations higher than 10^{-2} mol dm^{-3}, the emission intensity was observed to decrease with increasing concentration. Our results are consistent with this observation. The concentration of $Z-Ru(bpy)_3^{2+}$ samples studied in this work is higher than 10^{-2} M, and the observed decrease in emission intensity with an increase in concentration is comparable to that reported for cellophane-adsorbed $Ru(bpy)_3^{2+}$ (see I_{rel} in Table 1). Both Martin and Thomas attributed the variations in the emission energies and intensities to interactions between adjacent $Ru(bpy)_3^{2+}$ chromophores.

In discussing the origin of the spectral changes observed in the highly concentrated in $Z-Ru(bpy)_3$ samples, first the specifics of the zeolite matrix should be taken into consideration. Thus, as discussed at the end of the structural model section, the chromophores entrapped in the bulk of the zeolite particle have a different number of $Ru(bpy)_3^{2+}$molecules around them than those near the particle surface. Depending on how much the exciting light penetrates into the particle, different assemblies of $Ru(bpy)_3^{2+}$molecules are monitored and thus the issue of light penetration depth in zeolitic samples becomes important. If we assume that the extent of scattering of the exciting light from the zeolite framework is independent of the chromophore load,

the light absorption by the chromophore is the limiting factor for the depth of the light penetration. For the most concentrated sample studied here (0.46 mol dm^{-3} or 1 Ru/1.9 cages), it can be easily calculated (using Beer's law) that the light intensity drops to 10% of its original value within ~1.5 μm (assuming ϵ = 14 000[1b] for Z−$Ru(bpy)_3$), which is comparable with the zeolite particle size. Thus, for the highly concentrated samples, an increase in excitation power will probe more of the bulk of the zeolite particles. At low excitation powers, when only the surface (large fraction of isolated chromophores) of the highly loaded zeolite particles is probed, the spectral response should approach the most diluted samples (mostly isolated chromophores; see Table 3). Thus, under identical irradiation conditions, any differences in the spectral response of the diluted and concentrated samples must originate from the intermolecular interactions within the bulk of the highly loaded zeolite particle.

Using the emission data summarized in Table 1, along with the predictions of the shell model (Table 3), more detailed information can be deduced about the nature of the interactions responsible for the observed spectral changes. From inspection of Table 1, it is apparent that the most dramatic changes in the emission spectra are observed for the two most concentrated samples (1 Ru/4.4 cages and 1 Ru/1.9 cages). Interestingly, according to the prediction of the structural model (Table 3), for concentrations around 1 Ru/4.4 cages, the fraction of adjacent $Ru(bpy)_3^{2+}$−$Ru(bpy)_3^{2+}$ pairs starts to dominate the total population of the entrapped chromophores (shell "b" occupied by more than 60%). At a concentration of 1 Ru/ 1.9 cages, where the interaction effects are most apparent, ~95% of the chromophores occupy adjacent zeolite cages. On the basis of this correlation, we suggest that it is the interaction between $Ru(bpy)_3^{2+}$ complexes occupying adjacent zeolite cages that has a dominant effect on the observed spectral changes.

Excited-State Lifetimes. More quantitative information about the nature and extent of the interactions responsible for the changes in the electronic absorption and emission spectra can be obtained from the analysis of temporal decays of emission intensity by fitting the emission decay data to an adequate kinetic model. Possibly the most frequently used model for analysis of emission decays observed from chromophores entrapped in various heterogeneous media is the multiexponential model.

$$I = \sum_{i=1}^{n} I_{0i} \exp\left(-\frac{t}{\tau_i}\right) \qquad (1)$$

Kaneko and co-workers used the biexponential model to analyze the emission decay curves for $*Ru(bpy)_3^{2+}$ immobilized in a polysiloxane film.[17] Fitting the corresponding equation to experimental data, the authors extracted two lifetimes, $\tau_1 \approx 1$ μs and $\tau \approx 300$ ns, neither of which showed a dependence on the $Ru(bpy)_3^{2+}$ concentration. The contribution of the shorter component to the total emission, however, was observed to increase from ~20% at a concentration of 0.01 mol dm^{-3} to 50% at a concentration of 0.32 mol dm^{-3}. Although the origin of the two components was not discussed in detail, the authors implied that the longer component may be attributed to isolated $*Ru(bpy)_3^{2+}$ molecules and the shorter component to a $*Ru(bpy)_3^{2+}$ affected by a nearby ground-state $Ru(bpy)_3^{2+}$.

Another model suitable for analysis of kinetic behavior of systems in heterogeneous environments has been developed by Albery and co-workers.[18] The model is based on an assumption that there is a normal distribution ($\exp(-x^2)$) of free energy of activation (imposed on emitting species by the heterogeneous environment) about some mean $\Delta G^{\ddagger}$ (with distribution spread γ) rather than a single activation energy for all species. Both the dispersion (Albery's) model and the biexponential model were used by Martin[14] to study the effect of concentration on the excited-state lifetimes of $Ru(bpy)_3^{2+}$ incorporated into the layered colloid, ZrPS (zirconium phosphate sulfenyl phosphonate). Using the biexponential model, the only observed effect of increased $Ru(bpy)_3^{2+}$ concentration on the extracted parameters was the shortening of the longer component from 1100 to 666 ns with a 25-fold increase in the concentration of adsorbed $Ru(bpy)_3^{2+}$. The lifetime of the short component (~200 ns), as well as the relative contributions of each component to the total intensity, was unaffected by changes in $Ru(bpy)_3^{2+}$ concentration. Using the disperse kinetics model, Martin and co-workers derived a virtually linear decrease in average lifetime (going from τ = 800 ns to τ = 480 ns) with the 25-fold increase in concentration. The quenching mechanism responsible for the observed lifetime shortening was suggested to involve an external spin−orbit coupling effect (vide supra) between excited and ground-state chromophores.

A kinetic model for analysis of emission decays observed for the cellophane-adsorbed $*Ru(bpy)_3^{2+}$ was developed by Thomas and co-workers.[16] The authors assumed that adsorbed, excited $*Ru(bpy)_3^{2+}$ molecules can decay to the ground state either through intramolecular radiative and nonradiative pathways (as in solution) or their decay can be affected by a nearby ground- or excited-state molecule of $Ru(bpy)_3^{2+}$. Using this model, Thomas et al. have shown that, at low excitation powers, the excited $*Ru(bpy)_3^{2+}$ is quenched by a nearby ground-state molecule with a rate $k_q = (7.8 \pm 0.8) \times 10^6$ mol^{-1} dm^3 s^{-1} ($1/k_q = 128 \pm 15$ ns). The proposed mechanism involves an external spin−orbit coupling effect (vide supra) between the ground- and excited-state molecules, enhancing the intramolecular nonradiative decay of the latter. At high excitation powers, at which a sufficiently high population of the excited states is created, neighboring $*Ru(bpy)_3^{2+}$ molecules can interact. The proposed mechanism of interaction between two such excited states is the thermodynamically highly favorable triplet−triplet annihilation via electron transfer. The rate constant for this process extracted from the fits to emission data is $k_{TT} = (5.2 \pm 0.6) \times 10^7$ mol^{-1} dm^3 s^{-1} ($1/k_{TT} = 19 \pm 2$ ns). The evidence for the presence of this interaction mechanism is supported by the lifetime studies of $Ru(bpy)_3^{2+}$ dispersed in micelle solutions[19] where the triplet−triplet annihilation was documented to be a dominant quenching process, with the quenching being increasingly important with an increase in the number of $Ru(bpy)_3^{2+}$ molecules per micelle.

The kinetic expression derived by Thomas et al. is a mathematical representation of the situation where each excited molecule has an equal opportunity to decay to the ground state by any of the three possible pathways. This may be an accurate description of the processes occurring in highly concentrated liquid solutions, where the diffusion permits the contact between the molecules, and apparently also in the cellophane matrix, where the arrangement of adsorbed $Ru(bpy)_3^{2+}$ molecules over a continuum of intermolecular distances can mimic the diffusional freedom present in liquid solutions (if highly efficient energy and electron transfer is assumed). In the zeolite, only specific intermolecular distances between immobilized $Ru(bpy)_3^{2+}$ molecules are allowed. Thus, continuous kinetic models, such as the dispersion model developed by Albery and that by Thomas et al., are not adequate descriptions of the potential interactions between zeolite-entrapped $*Ru(bpy)_3^{2+}$ molecules. To account for specifics of the Y-zeolite topology,

we have developed a model in which the distinctive spatial arrangement of the entrapped emitters is taken into account.

3. Development of the Kinetic Model. Every zeolite-entrapped $Ru(bpy)_3^{2+}$ molecule can be assigned to one of three categories: (1) isolated molecules—separated from nearest molecule by a distance such that no significant interaction can occur (>60 Å); (2) Adjacent pair molecules—molecules forming an adjacent pair, with the pair being separated from other molecules by sufficient distance so that no interaction can occur; (3) the remaining molecules—separated from nearest molecule by 1, 2, ... *n* empty supercages (i.e., 9 Å, 13 Å, ...) and capable of some long-distance interaction.

This categorization is obviously valid only at concentrations sufficiently low such that no significant fraction of adjacent "triplets" or "quartuplets" is formed. Only at these low concentrations can relatively straightforward kinetic considerations be used in analysis of the experimental data.. Taking a ~10% fraction of adjacent multiplets as the highest acceptable limit, the samples with loadings of 1/66.7 to 1/7.5 fulfill the above requirement.[13] Consequently, only the emission decays recorded for the four most dilute zeolite samples were analyzed by the model developed in following sections.

The molecules belonging to the third category can, in principle, interact with their nearest neighbor (that is separated from them by one or more empty supercages). However, the intermolecular separation, ~9 Å (the minimal separation for molecules in this category), is sufficiently large so that the efficiency of long-range interaction mechanisms capable of causing any observable changes in the rate of the depopulation of the excited molecules is expected to be low.[20] Thus, when compared to strong interactions within adjacent pairs, these can be neglected. On the basis of this assumption, we divide the entrapped chromophores into two categories, isolated ions and adjacent pairs.

Within the limits of the above assumptions, three different emitting species can form inside the zeolite upon irradiation of $Z-Ru(bpy)_3^{2+}$:

(A) $Z-{}^*Ru(bpy)_3^{2+}$, isolated

(B) $Z-{}^*Ru(bpy)_3^{2+}\cdot Z-Ru(bpy)_3^{2+}$, adjacent excited-state−ground-state pair

(C) $Z-{}^*Ru(bpy)_3^{2+}\cdot Z-{}^*Ru(bpy)_3^{2+}$, adjacent excited-state−excited-state pair

For each of these species, possible decay mechanisms have been considered and corresponding kinetic expressions have been derived. These are discussed in the following paragraphs and summarized in Table 4.

3.A. Isolated $Z-{}^*Ru(bpy)_3^{2+}$. The population of those entrapped $*Ru(bpy)_3^{2+}$ molecules that are isolated from their nearest neighbors by a sufficient distance so that no interaction can occur will decay following first-order kinetics: $A \rightarrow B$, where $A = Z-*Ru(bpy)_3^{2+}$ and $B = Z-Ru(bpy)_3^{2+}$. The rate of decay of this population is determined by the sum of the individual rate constants for various decay pathways, with the corresponding overall rate constant typically expressed in the form

$$k_1 = k_r + k_{nr} + k' \exp(-\Delta E'/k_B T) \qquad (2)$$

In eq 2, the k_r and k_{nr} are radiative and nonradiative rate constants, respectively, and k' and $\Delta E'$ are the parameters connected with the population of a thermally activated state.

TABLE 4: Summary of the Mechanisms Possibly Contributing to the Depopulation of the Excited $Z-Ru(bpy)_3^{2+}$ and Corresponding Kinetic Expressions Used for the Analysis of Emission Decay Curves

A. Isolated $*Ru(bpy)_3^{2+}$	
$A \xrightarrow{k_1} B$	$I = I_0 \exp(-t/\tau_1)$
B. Adjacent ES−GS Pair	
(1) Nonradiative Decay Enhancement	
$A\cdot B \xrightarrow{k_2} B\cdot B$	$I = I_0 \exp(-t/\tau_2)$
C. Adjacent ES−ES Pair (Triplet−Triplet Annihilation)	
(1) Electron Transfer—Decay to Nonemitting Products	
$A\cdot A \xrightarrow{k_{el}} P$	$I = I_0 \exp(-t/\tau_{el})^a$
(2) Energy Transfer	
$^3A\cdot{}^3A \xrightarrow{k_{en}} (^1A\cdot B) \rightarrow {}^3A\cdot B \xrightarrow{k_2} B\cdot B$	$I = I_{01} \exp(-t/\tau_{en}) + I_{02} \exp(-t/\tau_2)^b$

^{a} $I_0 = k_r[A\cdot A]_0$, $\tau_{el} = 1/k_{el}$. ^{b} $I_{01} = k_r[A\cdot A]_0(1 + k_2/(k_2 - k_{en}))$, $I_{02} = k_r[A\cdot A]_0 k_{en}/(k_{en} - k_2)$, $\tau_{en} = 1/k_{en}$, $\tau_2 = 1/k_2$.[26]

As has been shown previously, the steric constraints imposed on the entrapped molecules by the zeolite cage affect the accessibility of the thermally populated states and thus the observed value of k_1.[8] In the case of $*Ru(bpy)_3^{2+}$, for example, the excited state is depopulated through a different thermally activated channel for the intrazeolitic complex than for $*Ru(bpy)_3^{2+}$ dissolved in propylene carbonate.[7b] However, at room temperature, the rate of $Z-*Ru(bpy)_3^{2+}$ depopulation is known to be comparable to the one observed for an aqueous solution of $*Ru(bpy)_3^{2+}$.[7b]

3.B. Adjacent $Z-{}^*Ru(bpy)_3^{2+}\cdot Z-Ru(bpy)_3^{2+}$ Interaction. Another category of emitting, zeolite-entrapped species consists of pairs of $Ru(bpy)_3^{2+}$ molecules entrapped in adjacent zeolite supercages with one member of the pair being excited. If the decay of the excited molecule to its ground state is affected by the presence of the ground-state molecule next to it, then the rate of the decay is different than in case A. We have considered several possible quenching mechanisms.

Nonradiative Decay Enhancement. Since the estimated distance between the complexes entrapped within the adjacent zeolite cages is ~1 Å, it is reasonable to assume that the adjacent chromophores can come into a contact through the 7 Å supercage window, distorting mutually their electronic structure and altering the electronic spectra. A decrease in the energy gap between the ground and excited state of the chromophore will lead to an enhancement of the nonradiative decay.[21] However, since the spectral perturbations that we observe in the $Z-Ru(bpy)_3^{2+}$ samples are very small, the energy gap effect on the kinetics of the excited-state depopulation is expected to be small.

Thomas[16] and Martin[14] have reported enhancement in the nonradiative decay of the immobilized $*Ru(bpy)_3^{2+}$ by a nearby ground-state $Ru(bpy)_3^{2+}$ and suggested an alternative mechanism (as compared energy gap effect) responsible for this observation. The enhancement has been attributed to "some sort of external spin−orbit coupling".[16] It is our understanding that these authors mean to imply a mechanism that is analogous to the previously described "external heavy atom effect". In that case, the heavy atom present in the vicinity of the chromophore enhances the extent of spin−orbit coupling within the chromophore, thus increasing the amount of singlet character of the excited state and in this way enhancing the rate of the "forbidden" triplet (ES)−singlet (GS) transition. Although the studies of Demas and Addington[22] of the "heavy atom effect" on the lifetime of $*Ru(bpy)^{3+}$ exposed to I^- and Ag^+ did not seem to confirm that this effect plays an important role in fluid solution, we

believe that the immobilization of the adjacent chromophores in zeolites (or other heterogeneous media) could enhance this effect and thus it becomes a possible quenching mechanism.

The net effect of a nonradiative decay enhancement by spin−orbit coupling is that the excited $*Ru(bpy)_3^{2+}$ chromophore, with the GS chromophore next to it, decays to the ground state more rapidly than the isolated $*Ru(bpy)_3^{2+}$. For the immobilized species, this process can be schematically written as

$$A{\cdot}B \rightarrow B{\cdot}B$$

where B·B represents two ground-state molecules immobilized in adjacent zeolite supercages and A·B represents an initial adjacent ES−GS pair.

Two additional interaction mechanisms within the ES−GS pair are energy and electron transfer. However, these two pathways are not affecting the emission decays (as the former does not lead to a change in the total population of the excited chromophores and latter is thermodynamically unfavorable) and thus are not considered in the following discussion.

*3.C. Adjacent Z−*Ru(bpy)$_3^{2+}$·Z−*Ru(bpy)$_3^{2+}$ Interaction (Triplet−Triplet Annihilation).* At sufficiently high photon flux (excitation power) and concentrations of the zeolite-entrapped $Ru(bpy)_3^{2+}$, there is an enhanced probability that two $Ru(bpy)_3^{2+}$ molecules entrapped within adjacent zeolite supercages will be excited at the same time (within the duration of a single laser pulse). Several authors[14,16,19] have suggested that two adjacent $*Ru(bpy)_3^{2+}$ molecules can interact quite efficiently and that such an interaction has a pronounced effect on the kinetics of the emission decay. Consequently, we have considered two possible interaction mechanisms within the doubly excited adjacent pair.

3.C.1. Electron-Transfer Quenching to Nonemitting Products. The electron transfer between two excited $*Ru(bpy)_3^{2+}$ molecules is thermodynamically quite favorable

$$*Ru(bpy)_3^{2+} + *Ru(bpy)_3^{2+} \rightarrow Ru(bpy)_3^{3+} + Ru(bpy)_3^{+}, \quad \Delta G^\circ = -1.7 \text{ eV}$$

and, in cases where two excited molecules are immobilized in adjacent zeolite supercages, this interaction can be expected to represent an important pathway for the depopulation of the excited $Z-*Ru(bpy)_3^{2+}$ molecules. The initial electron transfer can be subsequently followed by a highly exergonic back electron-transfer reaction[23]

$$Ru(bpy)_3^{3+} + Ru(bpy)_3^{+} \rightarrow 2Ru(bpy)_3^{2+}, \quad \Delta G^\circ = -2.6 \text{ eV}$$

or $Ru(bpy)_3^{3+}$ and/or $Ru(bpy)_3^{+}$ can possibly participate in other redox reactions (e.g., with intrazeolitic water).[24] A simple general kinetic scheme for the quenching of adjacent excited molecules by electron transfer leading to formation of nonemitting products has been suggested by Thomas:

$$A{\cdot}A \rightarrow P$$

where P represents an undefined nonemitting product. Prior to derivation of a corresponding kinetic expression, it is important to note that, within the concentration range studied, the members of the excited pair are assumed to be completely isolated (noninteracting) from any other nearby $Ru(bpy)_3^{2+}$ complex. Consequently, the rate of the depopulation of the A·A pair is determined exclusively by the rate of the electron transfer and is independent of variations in concentration or excitation power. Thus, although the electron transfer results in the simultaneous annihilation of two excited molecules, the decay of the excited pair to the ground state must still be treated as a first-order (rather than a second-order) process, with the rate constant corresponding to the rate at which the electron transfer occurs. The same logic was used in the development of the kinetic expression for the process discussed in following section.

3.C.2. Triplet−Triplet Annihilation via Energy Transfer. Hatchard and Parker[25] were the first to describe the effect of delayed fluorescence, observed from (otherwise nonfluorescing) anthracene and phenanthrene in ethanol. They proposed that the observed fluorescence is due to the following process:

$$\text{triplet} + \text{triplet} \rightarrow \text{singlet} + \text{ground state}$$

based on the fact that the observed fluorescence intensity was proportional to the square of the absorbed light intensity. The energetic requirement for this process to occur is that twice the energy of the triplet is larger than the energy of the singlet. In the case of $Ru(bpy)_3^{2+}$, this requirement is fulfilled ($E_{singlet} \simeq 22\,000$ cm^{-1}; $E_{triplet} \simeq 16\,000$ cm^{-1}).[1b] However, due to the very efficient singlet → triplet intersystem crossing, the acceptor $Ru(bpy)_3^{2+}$ complex will rapidly form a triplet state rather than decay via the singlet state (i.e., without possible observation of the singlet fluorescence). Thus, in the case of the $*Ru(bpy)_3^{2+}$−$*Ru(bpy)_3^{2+}$ pair, the net effect of such an interaction is the annihilation of the single excited $*Ru(bpy)_3^{2+}$ state followed by decay of the ES-GS pair according to the scheme

$$A{\cdot}A \rightarrow A{\cdot}B \rightarrow B{-}B$$

where A·A → A·B represents the triplet−triplet energy transfer followed by intersystem crossing. The depopulation mechanisms for the zeolite-entrapped $*Ru(bpy)_3^{2+}$ discussed in previous sections together with corresponding kinetic equations are summarized in Table 4.

To the extent that the three different emitting species present in the zeolite (i.e., isolated $*Ru(bpy)_3^{2+}$, ES−GS pair, ES−ES pair) are assumed to be noninteracting, the experimentally observed emission decay of $Z-*Ru(bpy)_3^{2+}$ is expected to be a composite of contributions of the three independent depopulation processes. Consequently, the fitting expression used for the analysis of the emission decays were constructed simply by adding kinetic terms summarized in Table 4. Thus, eq 3

$$I = I_{01}\exp\left(-\frac{t}{\tau_1}\right) + I_{02}\exp\left(-\frac{t}{\tau_2}\right) + I_{03}\exp\left(-\frac{t}{\tau_3}\right) \quad (3)$$

was constructed by adding the terms representing the depopulation of the isolated $Z-*Ru(bpy)_3^{2+}$ ions (term 1) with that representing the depopulation of the ES−GS adjacent pairs interacting via nonradiative decay enhancement (term 2) and with the one describing the depopulation of the ES−ES adjacent pairs (term 3). As is apparent from Table 4, the kinetic expressions for both the ES−ES decay mechanisms (electron transfer and energy transfer) considered in combination with expressions for ES−GS pairs and isolated $Z-*Ru(bpy)_3^{2+}$ ions result in a three-exponential expression (eq 3). The difference lies only in the interpretation of the preexponential factors I_{02} and I_{03} and the lifetime τ_3, and so the analysis of the emission decays alone cannot lead to distinguishing between the two annihilation mechanisms. While the energy transfer cannot be excluded based purely on thermodynamic considerations, in the following discussion it is assumed that the ES−ES pairs are annihilated via the electron transfer.

4. Analysis of Emission Decays. The emission decays observed from the four least concentrated $Z-*Ru(bpy)_3^{2+}$

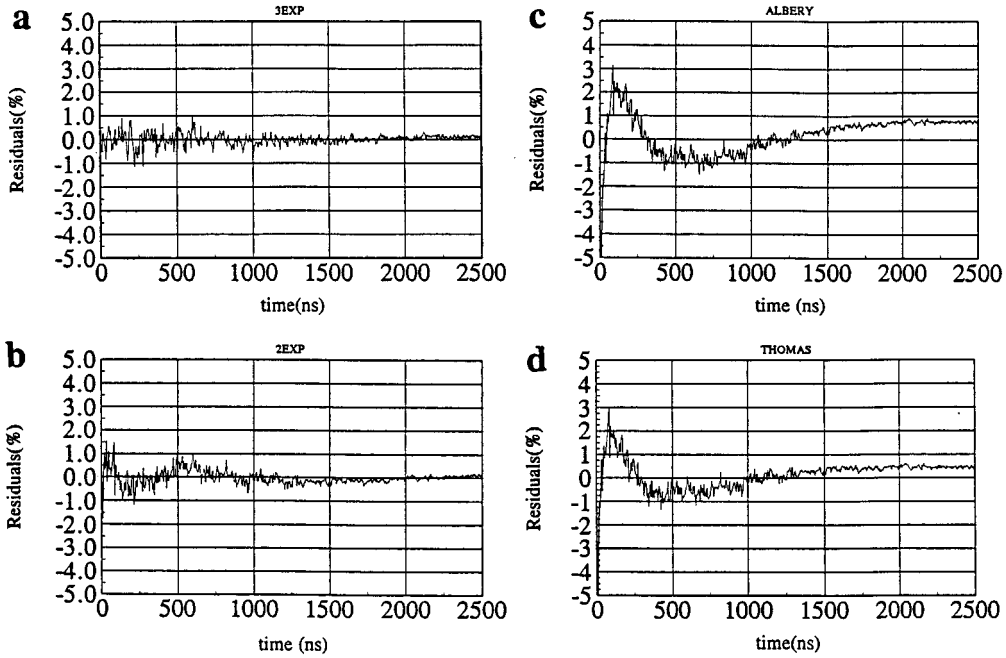

Figure 7. Comparison of results of fitting the experimental data to different kinetic models. Plotted residuals calculated according to the formula residuals (%) = 100 × ($I_{exp} - I_{calc}$): (a) fit to eq 3; (b) fit to biexponential model; (c) fit to dispersed model; (d) fit to model of Thomas et al. All the models were fit to experimental trace recorded for Z−*Ru(bpy)$_3$ (load of ∼1 Ru/7.5 supercages) at 50 mW, i.e., 2.5 mJ/pulse.

TABLE 5: Result of the Fit of Eq 3 to the Experimentally Observed Emission Decays

	laser power in mW (mJ/pulse)						
sample (load)	<0.5 (<0.025)	1 (0.05)	5 (0.25)	10 (0.5)	20 (1)	50 (2.5)	%ISO[a]
$[Ru(bpy)_3]Cl_2$[b]	585.6	585.7	580.5	573.7	561.2	557.8	
$Z-Ru(bpy)_3^{2+}$ (1/66.7)	613.9 (100)[c]	603.9 (96)	599.3 (94)	591.7 (92)	587.4 (89)	590.9 (90)	94.14%
		87.2 (4)	98.6 (6)	133.6 (5)	166.3 (7)	223.9 (7)	
				15.6 (3)	29.3 (4)	61.9 (3)	
$Z-Ru(bpy)_3^{2+}$ (1/29.7)	594.0 (96)	586.5 (87)	579.0 (84)	576.5 (84)	568.3 (80)	575.2 (82)	87.20%
	168.5 (4)	150.8 (9)	166.2 (11)	147.3 (12)	184.8 (14)	162.4 (11)	
		15.4 (4)	24.1 (5)	20.9 (4)	25.6 (6)	37.7 (7)	
$Z-Ru(bpy)_3^{2+}$ (1/14.0)	583.1 (95)	572.3 (84)	563.8 (78)	564.7 (73)	561.6 (73)	574.7 (71)	74.35%
	194.8 (5)	176.0 (10)	158.2 (15)	171.3 (17)	172.9 (18)	198.0 (19)	
		43.1 (6)	32.9 (7)	32.0 (10)	32.8 (9)	39.7 (10)	
$Z-Ru(bpy)_3^{2+}$ (1/7.5)	573.3 (97)	569.4 (79)	562.0 (73)	557.9 (67)	548.0 (69)	541.3 (68)	56.42%
	124.7 (3)	184.7 (13)	157.8 (18)	178.1 (20)	154.2 (20)	165.2 (19)	
		37.0 (8)	28.7 (9)	35.5 (13)	29.4 (11)	38.6 (13)	

[a] Probability for $Ru(bpy)_3^{2+}$ molecules to be isolated (i.e., 100 − % probability for population of shell b; see Table 2.). [b] Independently synthesized complex measured in H_2O. Concentration < 10^{-5}. [c] The number in parentheses represents relative contribution of given component to the total intensity (i.e., I_{01}, I_{01}, and I_{03}) in percent. In general $I_{0i} = k_r[*M]_0$, where $[*M]_0$ is fraction of emitting species at $T = 0$ and k_r is corresponding radiative rate constant. Assuming that intermolecular interactions do not affect the k_r significantly, the I_{0i} values represent directly the fraction of $*Ru(bpy)_3^{2+}$ belonging to A, A·B, or A·A category at $t = 0$. Estimated errors: lifetimes ±10 ns, relative contributions ±5%.

samples, (1 Ru/66.7 cages to 1 Ru/7.5 cages) measured at six different excitation powers (∼0.025−2.5 mJ), were analyzed. A sample plot of the residuals between the best fit to eq 3 and one of the experimentally observed emission curves is shown in Figure 7. Fits of comparable quality (i.e., the plot of residuals symmetrically distributed around zero value with deviations of ± 0.5%) were obtained for all curves analyzed using this equation. The parameters extracted from the fits of eq 3 to the experimental data are summarized in Table 5.

The following general trends can be found for this set of data. At very low powers and concentrations, the observed emission decay was satisfactorily fit by a simple monoexponential expression (i.e., first term in eq 3). Upon increasing the concentration (at low powers) or power (at lower concentrations), the use of a biexponential expression (the first two terms in eq 3) was necessary in order to obtain good fits to the experimental data. Finally, at high powers, eq 3 was needed to obtain acceptable fits. Using this approach, three distinct lifetime components were extracted: the long component with $\tau_1 \approx$ 560−610 ns, the intermediate component with $\tau_2 \approx$ 130−200 ns, and the short component with $\tau_3 \approx$ 20−40 ns.

The long component, attributed to the emission from isolated $*Ru(bpy)_3^{2+}$ molecules, shows only a slight dependence on the excitation power and the sample concentration; that is, the lifetime decreases by ∼20−30 ns across the studied concentration range and by the same amount across the studied power range. A practically identical power dependence of the lifetimes was observed for an aqueous solution of the $*Ru(bpy)_3^{2+}$ (data included in Table 5 for comparison). It was confirmed by lifetime studies performed at a lower repetition rate (e.g., 1 Hz) that these lifetime variations are due to the "global" sample heating effect. The extent of heating can be estimated by employing eq 3 and known values of the parameters k_r, k_{nr}, k', and $\Delta E'$ previously reported in the literature.[7b] Using this

approach, it is estimated that, for these zeolite samples, the lifetime variation of 20−30 ns corresponds to a temperature change in the chromophore environment of smaller than 2 °C.

In the case of the intermediate component, attributable to the emission from the ES−GS adjacent pairs, a temperature or concentration dependence of the lifetime is not apparent. However, any weak dependence may be hidden by the large fluctuations in the extracted values. These fluctuations are considered to be an artifact of the numerical fitting; that is, it is noted that when the relative contribution of an emission component decreased below 10%, there is a dramatic increase in the error associated with the corresponding lifetime value.

The lifetime value of the short component, associated with the emission from ES−ES adjacent pairs, presumably annihilated via the electron transfer, is in good agreement with the value reported for the same process in the case of the cellophane-adsorbed species (19 ± 2 ns).[16]

From the comparison of the relative contributions of each emitting component (values in parentheses), it is evident that the long component dominates the observed emission at all concentrations and all powers. This result is in overall agreement with the prediction of the shell model (see Table 3), according to which, in all the samples studied, the majority of the zeolite-entrapped $Ru(bpy)_3^{2+}$ (and thus also $*Ru(bpy)_3^{2+}$) molecules are isolated. The direct comparison of the relative contribution of the long component, extracted from the fits, with the theoretically calculated fraction of isolated molecules, %ISO (%ISO = 100 − %probability for formation of the adjacent pair—shell "b" in Table 3), indicates good agreement between the theory and the experiments done at powers exceeding 5 mW. At lower powers, the contribution of the isolated chromophores is considerably larger than that predicted by theory. In light of the discussion in previous sections, we suggest that this is a reflection of the different levels of penetration of the light into the sample at varying laser powers. The concentration of the transient $*Ru(bpy)_3^{2+}$ created by the laser pulse is at a maximum at the particle surface and presumably decays exponentially into the bulk of the particle. So, at low laser powers, it is the surface of the zeolite particle that is primarily being sampled, where the $Ru(bpy)_3^{2+}$ is more likely to be represented in our scheme as isolated species. At higher laser powers, the extent to which the bulk of the particle is being probed increases. Considering the fact that the internal surface area of zeolite particle is significantly higher than the external surface, at high laser powers, the signal from the bulk dominates the spectroscopic signal.

Conclusions

Over the past several years interest in the catalytic and photocatalytic applications of zeolite-entrapped metal complexes has increased and is likely to continue expanding. It is therefore important to understand not only the effect of the zeolite matrix on the chemical and photophysical properties of entrapped isolated complexes[3c,d,e,7,8] but also the nature and extent of interactions between complexes in close proximity. Employing a carefully prepared series of samples, wherein the concentrations of a well-characterized reference complex, $Ru(bpy)_3^{2+}$, have been increased incrementally so as to generate known fractions of adjacent pairs, the present study represents the first systematic attempt to thoroughly document such interactions.

The results of this study show that $Ru(bpy)_3^{2+}$ can be incorporated into Y-zeolite at high concentrations up to 0.46 mol dm^{-3} (1 Ru/1.9 cages) without significant contamination by reaction intermediates or starting materials. Within the concentration range 1 $Ru(bpy)_3^{2+}$/66.7 supercages to 1 $Ru(bpy)_3^{2+}$/1.9 supercages (i.e., 0.013−0.46 mol dm^{-3}), interactions between the zeolite-entrapped $Z-Ru(bpy)_3$ molecules have a profound effect on the spectroscopic properties of $Z-Ru(bpy)_3$. Specifically, a dramatic decrease in the emission intensity and complex kinetics of the $Z-*Ru(bpy)_3$ emission decay are observed as a result of these interactions. While the long-range (≥13 Å) interactions appear to be inefficient in zeolite, two different types of short-range (∼1 Å) interactions between $Ru(bpy)_3^{2+}$ ions occupying adjacent zeolite supercages have been identified. These have been associated with a nonradiative decay enhancement via ES−GS interaction and triplet−triplet annihilation via electron transfer (ES−ES interaction). While the rate of decay of the isolated $Z-*Ru(bpy)_3^{2+}$ molecules is comparable to that reported for the $Ru(bpy)_3^{2+}$ in aqueous solution ($\tau_1 \approx 614$ ns in zeolite vs $\tau_1 \approx 586$ ns in H_2O), the decay of the $Z-*Ru(bpy)_3^{2+}$ molecules forming an adjacent pair is much more rapid; that is, $\tau_2 \approx 160$ ns within an ES−GS pair and $\tau_3 \approx 30$ ns within an ES−ES pair.

Acknowledgment. The authors wish to thank Dr. Michael Slattery of the Department of Mathematics of Marquette University for his help in the development of the statistical structural model. This work was supported by grants from the Division of Chemical Sciences, U.S. Department of Energy (Grant DE-FG02-86ER13619 to J.R.K and Grant DE-FG02-90ER14105 to P.K.D).

Supporting Information Available: Additional information about the calculation of the distribution of the $Ru(bpy)_3^{2+}$ ions in the Y-zeolite (2 pages). Ordering information is given on any current masthead page.

References and Notes

(1) (a) Kalyanasundaram, K. *Coord. Chem. Rev.* **1982**, *46*, 219. (b) Juris, A.; Balzani, V.; Barigelletti, F.; Champagna S.; Belser, P.; Von Zelewski, A. *Coord. Chem. Rev.* **1988**, *84*, 85. (c) DeArmond, M. K.; Hanck, K. W.; Wertz, T. W. *Coord. Chem. Rev.* **1985**, *64*, 65.

(2) (a) Grätzel, M., Ed. *Energy Resources through Photochemistry and Catalysis*; Academic Press: New York, 1983. (b) Conolly, J. S., Ed. *Photochemical Conversion and Storage of Solar Energy*; Academic Press: New York, 1981. (c) Norris, J. R., Jr., Meisel, D., Eds. *Photochemical Energy Conversion*; Elsevier: Amsterdam, 1988.

(3) (a) Gafney, H. D. *Coord. Chem. Rev.* **1990**, *104*, 113. (b) Dutta, P. K.; Ledney, M. *Prog. Inorg. Chem.* **1997**, *44*, 209. (c) Turbeville, W.; Robins, D. S.; Dutta, P. K. *J. Phys. Chem.* **1992**, *96*, 5024. (d) Dutta, K. P.; Turbeville, W. *J. Phys. Chem.* **1992**, *96*, 9410. (e) Incavo, J. A.; Dutta, P. K. *J. Phys. Chem.* **1990**, *94*, 3075. (f) Kim, Y. I.; Mallouk, T. E. *J. Phys. Chem.* **1992**, *96*, 2879. (g) Kalyanasundaram, K. *Photochemistry of microheterogeneous systems*; Academic Press: New York, 1987.

(4) (a) Breck, D. W. *Zeolite Molecular Sieves*: *Structure Chemistry and Use*; Wiley: New York, 1974. (b) Weitcamp, J., Karge, H. G., Pfeifer, H., Holderich, W., Eds. *Zeolites and Related Materials: State of the Art*; Elsevier: Amsterdam, 1994.

(5) (a) DeWilde, W.; Peeters, G.; Lunsford, J. H. *J. Phys. Chem.* **1980**, *84*, 2306. (b) Quayle, W. H.; Lunsford, J. H. *Inorg. Chem.* **1982**, *21*, 97. (c) Lunsford, J. *ACS Symp. Ser.* **1977**, *40*, 473.

(6) (a) Dutta, P. K.; Incavo, J. A. *J. Phys. Chem.* **1987**, *91*, 4443. (b) Dutta, P. K.; Turbeville, W. *J. Phys. Chem.* **1992**, *96*, 9410. (c) Borja, M.; Dutta, P. K. *Nature* **1993**, *362*, 43. (d) Dutta, P. K.; Borja, M.; Ledney, M. *Sol. Energt Mater. Sol. Cells* **1995**, *38*, 239.

(7) (a) Maruszewski, K.; Strommen, D. P.; Handrich, K.; Kincaid, J. R. *Inorg. Chem.* **1991**, *30*, 4579. (b) Maruszewski, K.; Strommen, D. P.; Kincaid, J. R. *J. Am. Chem. Soc.* **1993**, *115*, 8345.

(8) Maruszewski, K.; Kincaid J. R. *Inorg. Chem.* **1995**, *34*, 2002.

(9) (a) Sykora, M.; Kincaid, J. R. *Nature* **1997**, *387*, 162. (b) Sykora, M.; Maruszewski, K.; Treffert-Ziemelis, S. M.; Kincaid J. R. *J. Am. Chem. Soc.* **1998**, *120*, 3490.

(10) Lainé, P.; Lanz, M.; Calzaferri, G. *Inorg. Chem.* **1996**, *35*, 3514.

(11) (a) One possibility is that complex kinetic behavior of $*Ru(bpy)_3^{2+}$ in Y-zeolite is simply a consequence of the local sample heating. We rejected

this possibility, considering the fact that the locally generated heat is expected to dissipate on the picosecond, rather than the nanosecond time scale;[11b] that is, on the time scale of the experiment, all the chromophores experience the same local temperature. It is important to note, however, that after equilibration the overall temperature of the sample can increase. This should, however, lead only to the increase in the overall rate of the emission decay and not appearance of the complex kinetics. Consequently, it is concluded here that the observed complex kinetics is not due to temperature effects but is rather due to specific interactions between the zeolite entrapped molecules of $Ru(bpy)_3^{2+}$. (b) Henry, E. R.; Eaton, W. A.; Hochstrasser, R. M. *Proc. Natl. Acad. Sci. U.S.A.* **1986**, *83*, 8982.

(12) Rillema, D. P.; Jones, D. S.; Levy, H. A. *J. Chem. Soc., Chem. Commun.* **1979**, 849.

(13) For details, see the Supporting Information.

(14) (a) Colón, J. L.; Yang, C.; Clearfield, A.; Martin, C. R. *J. Phys. Chem.* **1988**, *92*, 577. (b) Colón, J. L.; Yang, C.; Clearfield, A.; Martin, C. R. *J. Phys. Chem.* **1990**, *94*, 874.

(15) The concentrations of the $Ru(bpy)_3^{2+}$ in ZrPS are in the work of Martin et al. expressed as a fraction of the exchangeable $-SO_3^-$ sites occupied by the complex. The greater than 30 nm shift in absorption was observed between 1.7% and 8.7% loading. In the present work, the fractions of zeolite supercages occupied by $Ru(bpy)_3^{2+}$ are ~1.5%(1 Ru/66.7 cages) to ~52% (1 Ru/1.9 cages).

(16) Milosavijevic, B. H.; Thomas, J. K. *J. Phys. Chem.* **1983**, *87*, 616.

(17) Nagai, K.; Takamiya, N.; Kaneko, M. *J. Photochem. Photobiol. A: Chem.* **1994**, *84*, 271.

(18) Albery, W. J.; Bartlett, P. N.; Wilde, P. C.; Darwent, J. R. *J. Am. Chem. Soc.* **1985**, *107*, 1854.

(19) (a) Lachish, U.; Ottolenghi, M.; Rabani, J. *J. Am. Chem. Soc.* **1977**, *99*, 8062. (b) Baxendale, J. H.; Rodgers, M. A. J. *J. Phys. Chem.* **1982**, *86*, 4906.

(20) Kalyanasundaram, K. *Photochemistry of Polypyridine and Porphyrin Complexes*; Academic Press: San Diego, 1992; p 60.

(21) See, for example: (a) Caspar, J. V.; Meyer, T. J. *J. Phys. Chem.* **1983**, *87*, 952. (b) Caspar, J. V.; Kober, E. M.; Sullivan, B. P.; Meyer, T. J. *J. Am. Chem. Soc.* **1982**, *104*, 630.

(22) Demas, J. N.; Addington, M. C. *J. Am. Chem. Soc.* **1976**, *98*, 5800.

(23) (a) There is another thermodynamically favorable pathway for back electron transfer between $Ru(bpy)_3^{3+}$ and $Ru(bpy)_3^{+}$ i.e., via the reaction $Ru(bpy)_3^{3+} + Ru(bpy)_3^{+} \rightarrow {}^*Ru(bpy)_3^{2+} + Ru(bpy)_3^{2+}$; $\Delta G° = -0.41$ eV. In fact, this reaction pathway is kinetically more favorable than the reaction resulting in two ground-state $Ru(bpy)_3^{2+}$ ions, as demonstrated by efficient electrochemiluminescence in nonaqeous media.[23b] However, this reaction was found to be inhibited in an aqueous environment,[23c] and thus it is assumed here that only nonemitting products are formed in the reaction of $Ru(bpy)_3^{3+} + Ru(bpy)_3^{+}$ in zeolite. (b) Tokel, N. E.; Bard, A. J. *J. Am. Chem. Soc.* **1972**, *94*, 2862. (c) Rubinstein, I.; Bard, A. J. *J. Am. Chem. Soc.* **1980**, *102*, 6641.

(24) Ledney, M.; Dutta, P. K. *J. Am. Chem. Soc.* **1995**, *117*, 7687.

(25) Parker, C. A.; Hatchard, C. G. *J. Phys. Chem.* **1962**, *66*, 2506.

(26) Steinfeld, J. I.; Francisco, J. S.; Hase, W. L. *Chemical Kinetics and Dynamics*; Prentice Hall: Englewood Cliffs, 1989.